IEEE Access
Multidisciplinary | Rapid Review | Open Access Journal

Received 3 August 2022, accepted 12 August 2022, date of publication 16 August 2022, date of current version 26 August 2022.

Digital Object Identifier 10.1109/ACCESS.2022.3199065

RESEARCH ARTICLE

Equivalent Circuit Modeling and Experimental Analysis of Low Frequency Metamaterial for Efficient Wireless Power Transfer

WEBSTER ADEPOJU[1], (Graduate Student Member, IEEE), INDRANIL BHATTACHARYA[1], (Senior Member, IEEE), MARY SANYAOLU[2], AND EBRAHIM NASR ESFAHANI[1], (Student Member, IEEE)

[1]Department of Electrical and Computer Engineering, Tennessee Technological University, Cookeville, TN 38505, USA
[2]GasFleet Engineering, Lagos, Lagos State 100267, Nigeria

Corresponding authors: Webster Adepoju (woadepoju42@tntech.edu) and Indranil Bhattacharya (ibhattacharya@tntech.edu)

ABSTRACT This study proposes a low-frequency metamaterial(MM) coupled with an equivalent circuit model to emulate the behavior of an MM-based Wireless Power Transfer (WPT) system. For this purpose, the electromagnetic simulation and Finite Element Analysis (FEA) of the proposed MM-based WPT system are performed in ANSYS three-dimensional (3D) High-Frequency Structured Simulator (HFSS). In addition, numerical analysis of the circuit design of the proposed structure is performed in a MATLAB simulation environment to evaluate its transfer characteristics. While some methods, including effective medium theory and transmission line circuit model, have been exploited to explain the physical mechanism of MM-based WPT systems, some of the reactive parameters and the fundamental physical interpretation have not been clearly expounded. In contrast to existing theoretical models, the proposed approach focuses on the effect of system parameters of the MM and transfer coils on transfer characteristics, coupled with its effectiveness in analyzing complex circuits. A design prototype is fabricated for experimental measurement of power transfer efficiency and medium parameters using the KeySight ENA 5061 vector network analyzer (VNA), confirming the validity of the proposed design. The excellent efficiency enhancement and mutual coupling make the design an attractive solution for WPT applications. A close agreement of the experimental results and numerical simulation validates the accuracy of the analytical model.

INDEX TERMS Wireless power transfer, finite element analysis (FEA), metamaterial, power transfer efficiency, ANSYS, high frequency structure simulator (HFSS), equivalent circuit model, transfer function.

I. INTRODUCTION

In the last few decades, immense research effort has culminated in a broader utilization of Wireless Power Transfer (WPT) system as an alternative power transmission mechanism in mobile computing [1], wireless charging of biomedical body implants [2], consumer electronics and wireless charging of Electric Vehicles (EV) [3], [4]. However, despite its increasing penetration, reliability concerns stemming from high power dissipation, leakage Electromagnetic Field (EMF), and low power transmission efficiency (PTE) for wide range WPT systems remain largely unresolved. In light of this, attention has shifted to metamaterial (MM) as a preferred candidate for range extension and performance enhancement of WPT systems. As exhibited in Figure 1, MM(s) are generally categorized as double negative (DNG)/left-handed media, μ-negative (μNG) or ϵ-negative (ϵNG) depending on the polarity of medium properties, including the refractive index (n), effective permeability (μ_f), effective permittivity (ϵ_f), and the amplitude of magneto-inductive wave (MIW). Double-negative/ negative index MMs (NIMs) are the first and most investigated of all MM structures and they typify a generic description for left handed materials, exhibiting negative refractive index,

The associate editor coordinating the review of this manuscript and approving it for publication was Luyu Zhao.

n, as depicted in (1), and hence supports perfect lensing ($\epsilon_f = -1$, and, $\mu_f = -1$) [5].

$$n = -\sqrt{\mu_f \epsilon_f} \tag{1}$$

When operated at resonance, electromagnetic (EM) fields are confined inside the resonators, leading to a periodic exchange of electric and magnetic energy. Outside the resonators, however, the EM fields decay evanescently and do not carry away energy unless coupled to the tail of the evanescent wave of another resonator. With an NIM, the amplitude of evanescent waves can be enhanced such that the distance between the two resonators is small. The strategy for designing an NIM borders on reconstructing and modulating its structural properties, including effective permeability (μ_f), and effective permittivity (ϵ_f) coupled with optimization of physical parameters such that the reconstructed MM exhibits left-handed characteristics ($\mu_f < 0$ and $\epsilon_f < 0$). Meanwhile, the evanescent wave amplification property of MM is of significant interest in this study. This finds explanation in the fact that magnetic resonance coupling depends on evanescent wave amplification of near magnetic field. Considering the fact that inductive WPT and evanescent wave amplifier harness only the magnetic field for power transfer, it goes without saying that a negative real part of effective permeability ($\mu_f < 0$) is a satisfactory requirement for the material under test to achieve negative refractive index [6]. Besides, it is worth mentioning that for practical realization of a low frequency MM design, the MM unit cell must satisfy homogenization criterion, which stipulates that for effective medium properties to be valid, the sample size (l) of the unit cell must be extremely small in comparison to its wavelength ($l \ll \lambda$) at the resonant operating frequency [6], [7].

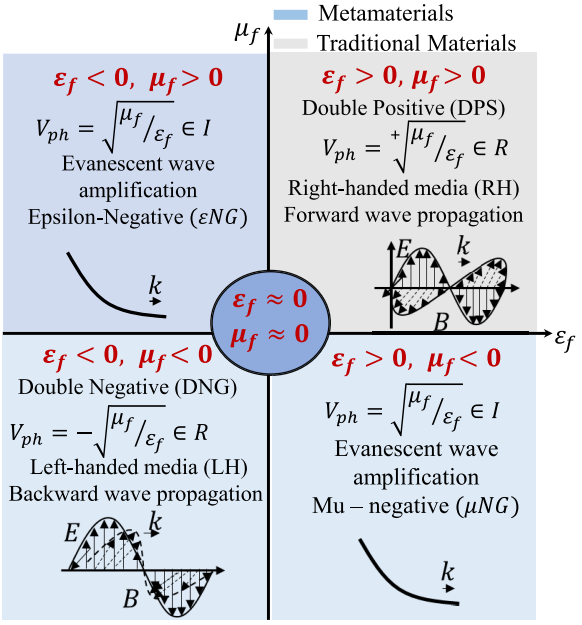

FIGURE 1. Classification of metamaterial (MM) based on the polarity of effective permeability, (μ_f) and effective permittivity (ϵ_f). E, B, k, V_{ph} denote the electric field, magnetic filed, wave number, and phase velocity, respectively.

Following these issues, this manuscript proposes a low frequency metamaterial (MM) coupled with an equivalent circuit model for exploring the transfer characteristics of a MM-based WPT system. While several methods, including interference theory [8], [9], transmission line circuit model [10], [11], and effective medium theory [12] have been widely exploited in literature to explain the physics of MM-based WPT systems, some of its reactive parameters, and the basic physical interpretation have not been clearly expounded. In contrast to existing theoretical models, the proposed methodology focuses on the effect of system parameters and transfer coils on the system transfer functions, which is pertinent in analyzing complex systems. Besides, most existing MM(s) in the literature suffer from high power dissipation, stemming from their inherently high microwave and radio frequencies [13], [14], which imposes high switching losses on the power switches while also subjecting the passive components to high voltage and current stresses [15], [16], [17]. Essentially, the proposed MM-slab consists of a 4×4 periodic array of MM unit cell exemplified in Figure 3. Moreover, a four-coil structure depicted in Figure 2, comprising the drive coil (dr), transmitting coil (Tx), receiving coil (Rx), and load coil (l) is utilized for theoretical analysis, the MM-slab being posited between the Tx and Rx coils. Specifically, the main contributions of this manuscript are presented below:

i designs a low frequency metamaterial (MM) sample for enhancing the efficiency of a WPT system
ii develops an equivalent circuit model for emulating the transfer characteristics of MM-based WPT system.
iii designs an experimental test-bed for evaluation of prototype sample while analyzing measurement results to validate the accuracy of the analytical model

The rest of the paper is presented as follows: Section II comprehensively describes the physics-based model derivation and equivalent circuit analysis of the proposed MM-based WPT structure. Moreover, the sensitivity of the proposed system to lateral and angular misalignments is concretely investigated. Further, section III explicitly analyzes the electromagnetic simulation, characterization, and parameter extraction of the proposed MM. In Section IV, efficiency and mutual impedance measurements are conducted on a fabricated prototype to ascertain the performance-enhancing capability of the proposed design. By leveraging printed circuit board technology (PCB), the unit cell is fabricated into a planar structure of a 4×4 periodic array to form an MM-slab.

II. PHYSICS BASED MODELING AND ANALYSIS OF THE PROPOSED DESIGN

A. EQUIVALENT CIRCUIT MODELING OF THE PROPOSED METAMATERIAL BASED WPT SYSTEM

In order to simplify the equivalent circuit model of the proposed structure, the circuit schematic of the proposed MM unit cell is modeled into coupling coils as seen in Figure 3(a).

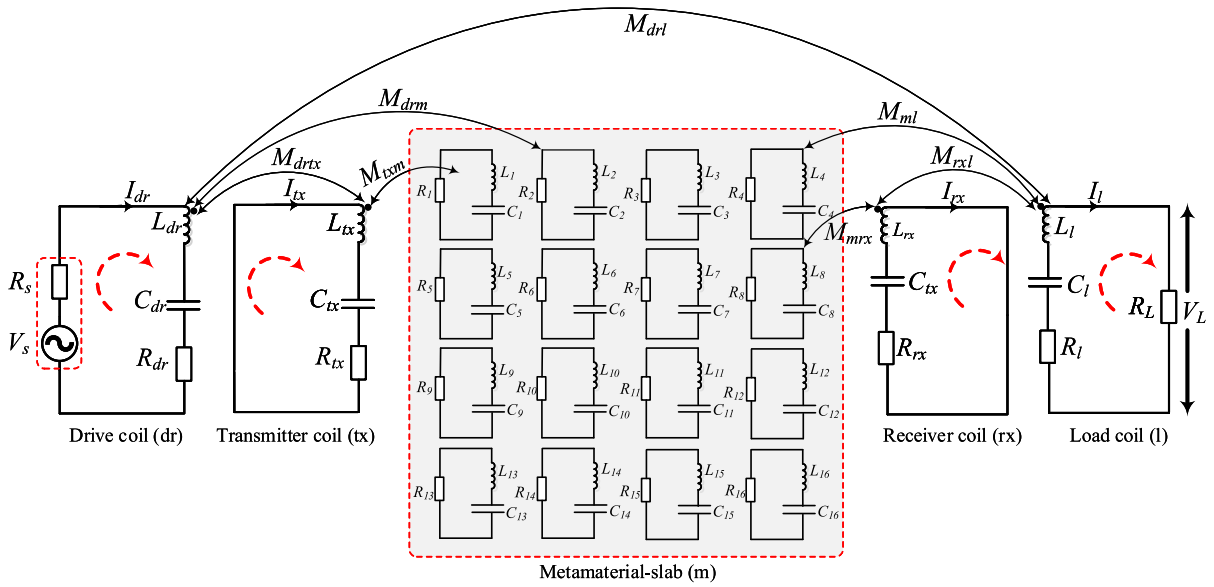

FIGURE 2. Equivalent circuit schematic of the proposed metamaterial (MM) WPT system based on four coil structure. The metamaterial slab consists of a 4 × 4 periodic array of MM unit cells in Fig. 3.

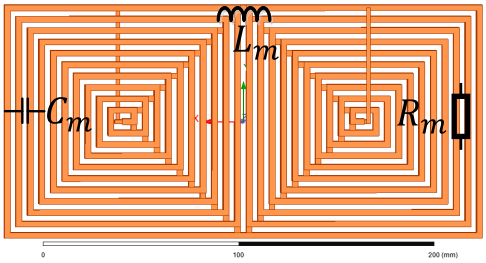

(a) CAD model of the proposed metamaterial (MM) unit cell based on ANSYS HFSS

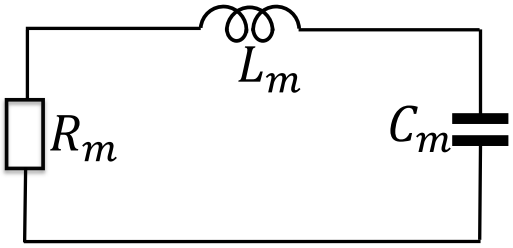

(b) Equivalent lumped resonant RLC circuit representation of the proposed MM in Figure 3(a)

FIGURE 3. Front view of proposed MM unit cell as designed in ANSYS HFSS.

Based on [18] and [19], each unit cell can be represented as a resistance-inductor-capacitor (RLC) resonant circuit exhibited in Figure 3(b) where L_m, C_m, and R_m are the lumped circuit inductance, capacitance and resistance of the unit cell, respectively, and the subscript $m = 1, 2, 3 \ldots 16$ denotes the number of resonant unit cells in the MM-slab. As shown in (2), the resistive component, R_m consists of the ohmic loss (R_o) and dielectric loss (R_d) due to the dielectric substrate.

$$R_m = R_o + R_d \tag{2}$$

Similarly, the capacitive component has been modeled as the sum of the stray capacitance, (C_s), and compensation capacitor, C_{com}, as exhibited in Eq. (3).

$$C_m = C_s + C_{com} \tag{3}$$

It is worth stating that the resonant frequency of the MM structure can be adjusted and tuned by varying the value of the compensation capacitor (C_{com}), accordingly, leading to optimized performance of the WPT system. Further, the metamaterial slab, which is posited between the *Tx* and *Rx* coils in Figure 2 is designed based on a 4 × 4 periodic array of the MM unit cell in Figure 3. Essentially, such a loosely disconnected array of metamaterial cells can be considered as a multiple repeater coils or booster network for achieving evanescent wave amplification and coupling of near magnetic field. Besides, the current flow through each unit cell of the MM-slab can be assumed identical and in phase while representing the entire system as a lump circuit model, in which the distribution of the parameters is ignored. Moreover, the parameters of the four coil structure in Figure 2 is expounded as follows:

- L_{dr}, C_{dr} and R_{dr} are the self-inductance, capacitance and resistance of the driver coil, respectively.
- L_{tx}, C_{tx} and R_{tx} are the self-inductance, capacitance and resistance of the transmitting coil, respectively.
- L_{rx}, C_{rx} and R_{rx} are the self-inductance, capacitance and resistance of the receiving coil, respectively.
- L_l, C_l and R_l are the self-inductance, capacitance and resistance of the load coil, respectively.
- L_m, C_m and R_m are the self-inductance, capacitance and resistance of the metamaterial, respectively.
- M_{drtx} is the mutual-inductance between the driver coil and transmitting coil.
- M_{drm} is the mutual-inductance between the driver coil and each MM-slab.
- M_{txm} is the mutual-inductance between the transmitting coil and MM-slab.

- ◇ M_{mrx} is the mutual-inductance between the MM-slab and receiving coil.
- ◇ M_{ml} is the mutual-inductance between the MM-slab and load coil.

Meanwhile, Z_{dr}, Z_{tx}, Z_{rx}, Z_l and Z_m denote the impedance of the driver coil, transmitter coil, receiver coil, load coil and each MM unit cell, respectively. Similarly, I_{dr}, I_{tx}, I_{rx}, I_l and I_m symbolize the current flowing through the driver coil (dr) transmitter coil (tx), receiver coil (rx), load coil (l) and each MM unit cell, respectively. By leveraging the concept of coupling theory and applying Kirchhoff's Voltage Law (KVL) to the equivalent WPT circuit in Figure 2, the individual impedance of the resonant coils and the overall circuit expression of the WPT system can be analyzed as demonstrated in Eq. (4) and Eq. (5), respectively.

$$\begin{cases} Z_{tx} = R_{tx} + j\left(\omega L_{tx} - \dfrac{1}{\omega C_{tx}}\right) \\ Z_{rx} = R_{rx} + j\left(\omega L_{rx} - \dfrac{1}{\omega C_{rx}}\right) \\ Z_{dr} = R_{dr} + j\left(\omega L_{dr} - \dfrac{1}{\omega C_{dr}}\right) \\ Z_l = R_L + R_l + j\left(\omega L_L - \dfrac{1}{\omega C_L}\right) \\ Z_m = R_m + j\left(\omega L_m - \dfrac{1}{\omega C_m}\right) \end{cases} \tag{4}$$

$$\begin{cases} V_s = (R_s + Z_{dr})I_{dr} + j\omega M_{drtx} I_{tx} + j\omega \sum_{m=1}^{16} M_{drm} I_m + \\ \qquad \cdots + j\omega M_{drl} I_l \\ 0 = j\omega M_{drtx} I_{dr} + Z_{tx} I_{tx} + j\omega \sum_{m=1}^{16} M_{txm} I_m + \\ \qquad \cdots + j\omega M_{txl} I_l \\ 0 = j\omega \sum_{m=1}^{16} \Big(M_{drm} I_{dr} + M_{txm} I_{tx} + Z_m I_m + \\ \qquad \cdots + M_{ml} I_l \Big) \\ 0 = j\omega M_{drl} I_{dr} + j\omega M_{txl} I_{tx} + j\omega \sum_{m=1}^{16} M_{ml} I_m + \\ \qquad \cdots + (R_L + Z_l) I_l \end{cases} \tag{5}$$

where m (1,2,3…16) denotes the number of resonant metamaterial unit cells. Converting Eq. (5) to matrix form culminates in

$$\begin{bmatrix} V_S \\ 0 \\ 0 \\ \vdots \\ 0 \end{bmatrix} = \begin{bmatrix} R_s + Z_{dr} & jwM_{drtx} & jwM_{drm} & \cdots & jwM_{drl} \\ jwM_{drtx} & Z_{tx} & jwM_{txm} & \cdots & jwM_{txl} \\ jwM_{drm} & jwM_{txm} & Z_m & \cdots & jwM_{ml} \\ \vdots & \vdots & \vdots & & \vdots \\ jwM_{drl} & jwM_{txl} & jwM_{ml} & \cdots & R_L + Z_l \end{bmatrix} \times \begin{bmatrix} I_{dr} \\ I_{tx} \\ I_m \\ \vdots \\ I_l \end{bmatrix} \tag{6}$$

where $\omega = 2\pi F_r$ in rad/s and F_r is the resonant frequency of the metamaterial unit cell as elicited in Eq. (7).

$$F_r = \frac{1}{2\pi\sqrt{L_m C_m}} \tag{7}$$

Thus, the current flowing through each resonant coil and the MM-slab can be evaluated based on a numerical solution of Eq. (6) in MATLAB simulation environment. Given the weak magnetic coupling between two non-adjacent coils, the associated mutual inductances M_{drm}, M_{txrx}, M_{ml}, and M_{drl} can be effectively neglected, as depicted in Eq. (8)

$$M_{drm} = M_{txrx} = M_{ml} = M_{drl} = 0 \tag{8}$$

As would later be described in section IV, the relevant mutual inductances; M_{drtx}, M_{txm}, M_{mrx}, and M_{rxl}, are extracted based on the electromagnetic finite element simulation of the MM WPT design. In addition, the calculation results are determined consistent with the theoretical analysis of Eq. (4) and Eq. (5). Further, the essential components (capacitor, inductance and resistance) are obtained in line with [20]. Using the four KVL equations in (4) and the circuit matrix model in Eq. (6) and harnessing the numerical method presented in [21] in a Matlab simulation environment, the resulting voltage transfer function is evaluated as in Eq. (9)

$$\frac{V_L}{V_S} = \frac{\omega^3 L_{tx} L_{rx} R_L \sqrt{L_{dr} L_l}}{Z_{dr} Z_{tx} Z_{rx} Z_l + \omega^2 \big(L_{dr} L_{rx} Z_{rx} Z_l + L_{tx} L_{rx} Z_{dr} Z_l + L_{rx} L_l Z_{dr} Z_{tx} \big) + \omega^4 \big(L_{dr} L_{tx} L_{rx} L_l \big)} \tag{9}$$

Therefore, the load voltage, V_L, can be evaluated by substituting the four KVL expressions in Eq. (4) into Eq. (9). In agreement with [20] and [21] coupled with the expression in Eq. (9), the equivalent transmission scattering parameter, S_{21}, is evaluated as shown in Eq. (10)

$$S_{21} = 2\frac{V_L}{V_S}\left(\frac{R_S}{R_L}\right)^{\frac{1}{2}} \tag{10}$$

To achieve impedance matching and maximum PTE, both the source resistance (R_s), and load resistance (R_L) are assumed to be 50Ω [8]. Alternatively, impedance matching can be realized by a simple adjustment of the distance between the drive coil (dr) and transmitter (tx), as well as the distance between the receiver (rx) and load (l) coils.

III. METAMATERIAL SIMULATION, CHARACTERIZATION AND PARAMETER EXTRACTION

A. ELECTROMAGNETIC (EM) sIMULATION AND FINITE ELEMENT ANALYSIS (FEA)

An ANSYS HFSS model of the proposed four coil WPT structure with and without MM-slab is exemplified in Figure 4(a) and Figure 4(b), respectively. In order to validate the accuracy of the proposed circuit equations, the PTE and transmission coefficient (S_{21}) of the WPT system are investigated based on a comparative analysis of the EM-simulation and theoretical model derived in section II. Using the concept of Finite Element Analysis (FEA), both designs are simulated

TABLE 1. Parameter specification of MM-based WPT model.

Parameter	Symbol	Unit	Value
Inductance	L_{dr}, L_l L_m	mH μH	0.7 1.49
Capacitance	C_m	pF	40
Compensation Capacitance	C_{com}	pF	600
Resistance	R_s, R_l R_m	Ω pF	50 40
Solution Frequency	F_{WPT}	MHz	6.78
Resonant Frequency	F_r	kHz	743.5

in ANSYS HFSS to extract the medium parameters. The resonant coils are made of three turns of 26AWG copper wire gauge, each having a diameter of 42*mm* while the metamaterial is designed with Litz wire. Litz wire is preferred because it exhibits minimal saturation and relaxation at high frequency, an important requirement for mitigating power loss and enhancing PTE [22]. Further, the complete WPT set up was excited at 6.78MHz solution frequency in compliance with International Commission on Non-Ionizing Radiation Protection (ICNIRP) which stipulates a leakage EMF $\leq 270mG$ for human safety [23], [24].

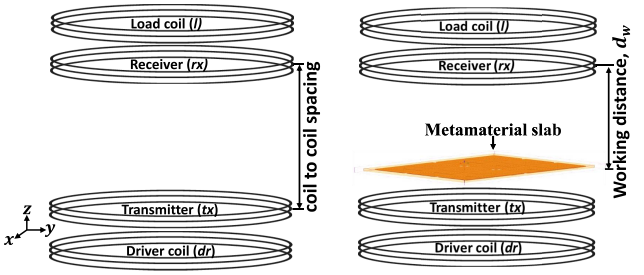

(a) Without metamaterial (MM) (b) With metamaterial (MM)

FIGURE 4. ANSYS HFSS simulation model of the proposed four coil WPT system (a) without metamaterial slab (b) with metamaterial slab.

Meanwhile, the simulation parameters in Table 1 are chosen in conformity with IEEE standard criterion, which specifies a 5% maximum harmonic content for ripple minimization [25]. The simulation was performed starting with the original system (without MM-slab). Going forward, the MM-slab was integrated with the WPT system to enhance mutual coupling, placing the slab 1mm away from the transmitter to preserve the working distance while fixing the useful working distance at 50*mm*. The resulting magnetic field distribution based on the EM-simulation with and without MM-slab is depicted in Figure 5a and Figure 12(b), respectively. Ostensibly, the distributed magnetic field using metamaterial is highly concentrated and about $\times 10$ denser compared to the original Tx/Rx coils without metamaterial. The observed performance enhancement due to the inclusion of MM can be attributed to its capability for evanescent wave amplification which essentially confines near magnetic field and leakage flux lines while also converging the traveling magnetic flux lines towards the *rx* coil. In addition, it is

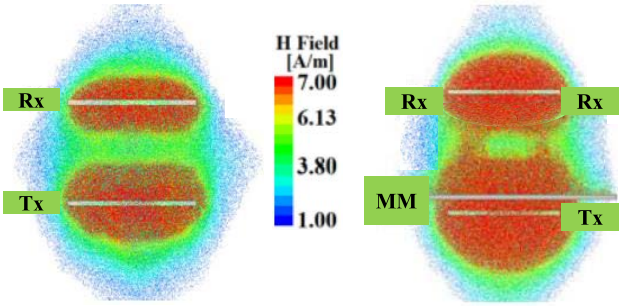

(a) Without metamaterial (b) With metamaterial

FIGURE 5. ANSYS HFSS simulation of the proposed metamaterial-based WPT system, showing the distribution of magnetic field (a) without metamaterial slab (b) with metamaterial slab.

worth stating that as the distance between the *Tx* and *Rx* coils increases, the distributed magnetic flux diverges, leading to power loss and a degradation in overall power transmission efficiency (PTE)

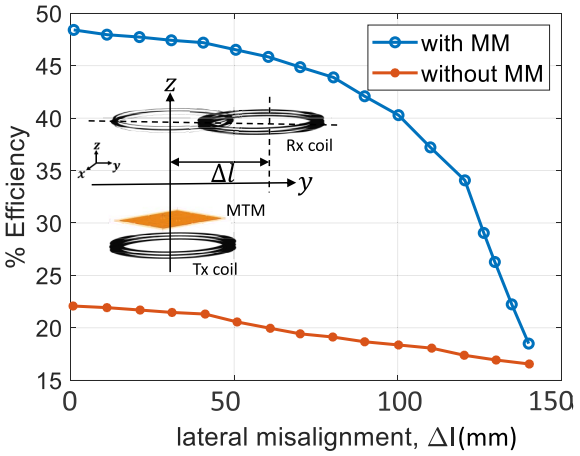

FIGURE 6. Lateral misalignment based analysis of power transfer efficiency of a conventional and metamaterial based wireless power transfer system.

B. SENSITIVITY ANALYSIS: LATERAL MISALIGNMEMT (ΔL) AND ANGULAR MISALIGNMENT (θ)

In this section, we investigate the effect of lateral and angular misalignment on the efficiency of the proposed WPT system in the presence and absence of metamaterial. Figure 6 and Figure 7 explicitly demonstrate the simulation waveform of the proposed structure for lateral and angular misalignment, respectively. Apparently, when the *Rx*-coil is subjected to 75% lateral misalignment relative to the *Tx*-coil and MM-slab, a diminution in PTE for each lateral displacement is observed. In perspective, for a lateral displacement of 50*mm* (based on Figure 6), the waveform shows an efficiency of 21% and 47% for the MM-based and non-MM based WPT design, respectively. The above results essentially underscores the performance enhancing capability of the proposed

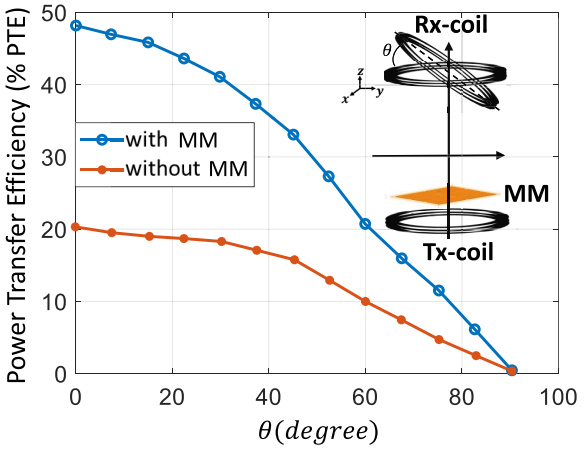

FIGURE 7. Angular misalignment based analysis of power transfer efficiency of a conventional and metamaterial based WPT system.

metamaterial. Moreover, considering an angular misalignment (θ) of 40^o as a case in point for both WPT scenarios (based on Figure 7), it is apparent that the WPT system using MM achieves a 28% improvement in efficiency. By and large, the WPT system using MM demonstrates a higher efficiency and an improved performance for all lateral and angular misalignment conditions compared to the original system without MM.

C. MAGNETIC PERMEABILITY EXTRACTION

The extraction of medium parameters is investigated using the set-up in Figure 2. It consists of four mutually coupled coils, where the reference coil (driver coil, dr) is actively driven by a voltage pulse from a function generator, creating a transient magnetic field, while measuring the induced time dependent voltage at the terminal of the pick up coil based on mutual coupling. Consistent with the work in [17], the voltage across the drive coil and pick-up coils can be expressed as

$$\begin{cases} V_s(t) = -\mu_o \dfrac{\partial}{\partial t}\hat{H}_z.dS \\ V_L(t) = -\mu_o\mu_f \dfrac{\partial}{\partial t}\hat{H}_z.dS \end{cases} \tag{11}$$

where dS is the area of the receiver coil, μ_o is the free space permeability, and H_z is the $\hat{z}$ component of the magnetic field (H-field). Essentially, the effective permeability, μ_f, of the samples can be trivially derived from Eq. (11), when the areas, dS of the receiver coil, and MM sample are made equal.

$$\widetilde{\mu}_f(\omega) = \frac{\widehat{F}[V_L(t)]}{\widehat{F}[V_s(t)]} \tag{12}$$

where $\widehat{F}$ is a complex Fourier transform. It should be noted that the validity of (12) is contingent on the assumption that the H-field between the MM sample and reference/source cancels out. Concretely, the effective permeability (μ_f) in Eq. (12) can be solved numerically in MATLAB simulation environment, applying it directly to the MM-based WPT system in Figure 4(b).

IV. EFFICIENCY ANALYSIS

In general, the efficiency (η) of a two-coil WPT system is often written in terms of the inductance of the transmitter (tx) and receiver (rx), and the coupling coefficient (k) between them.

$$\eta = \frac{-4\pi^2 F_r^2 k^2 L_{tx} L_{rx}}{R_L R_s + 4\pi^2 F_r^2 k^2 L_{tx} L_{rx}} \tag{13}$$

where L_{tx} and L_{rx} are the coil's self-inductance and F_r is the resonant operating frequency [26]. In this manuscript, however, a different approach for evaluating the WPT efficiency is explored. Consider a pair of inductively coupled coils connected to port 1 and port 2 of a Vector Network Analyzer (VNA) as shown in Figure 8(a). The two-port Z-parameters (Z_{11}, Z_{22}, and Z_c) are extracted using the schematic in Figure 8(b), where Z_{11} and Z_{22} represent the impedance at each port when the remaining port is opened, whereas Z_c is the mutual impedance, representing the shared magnetic field between the resonant coils. Subsequently, the extracted Z-parameters are harnessed in the equivalent circuit shown in Figure 8(b). Given that there is no extant assumptions regarding the nature of Z_c, the validity of the 2-port model in Figure 9 remains intact even when a metamaterial or passive metasurface is inserted between the tx and rx coils.

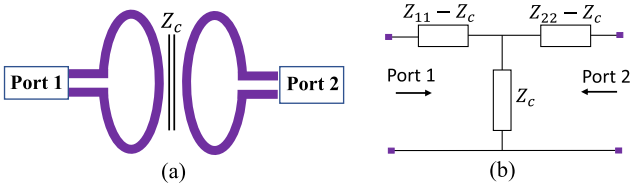

FIGURE 8. Schematic of two-inductively coupled coils (a) diagrammatic set-up (b) equivalent circuit representation.

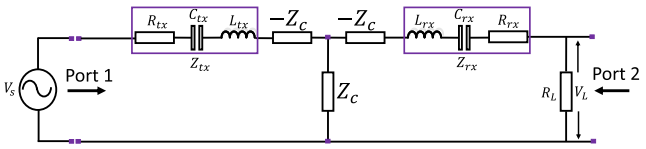

FIGURE 9. Schematic diagram of equivalent 2-port circuit, describing the WPT test case. The useful load (R_s) at the receiver is in series configuration.

Consequently, the equivalent circuits of the two coupled coils are used to construct the resonant circuit diagram depicted in Figure 9. Thus, the overall impedance of the tx and rx coils based on the two-port network in Figure 9 is expressed as in Eq. (14).

$$Z_k = R_k + j\left(\omega L_k - \frac{1}{\omega C_k}\right) \quad k \in \{tx, rx\} \tag{14}$$

where L_k is the inductance of the kth coil; C_k- the kth coil resonating capacitor, and R_k- total parasitic resistance of the sub-circuit. Further, the effective Z-parameters, $Z_{11,ef}$ and $Z_{21,ef}$, of the WPT design can be computed as indicated in

TABLE 2. Parameter specification for experimental design.

Parameter	Metamaterial	Transmitter	Receiver
Substrate	FR4	PLA	PLA
Turns	10	5	5
Copper wire guage	-	26 AWG	26 AWG
Trace Width	$2mm$	$2mm$	$2mm$
Outer diameter	N/A	$30mm$	$30mm$
Inner diameter	N/A	$20mm$	$20mm$
Size	$64 \times 32 \times 3mm^3$	N/A	N/A
Capacitance (C_{com})	$600pF$	N/A	N/A

Eq. (15)

$$\begin{cases} Z_{11,ef} = (Z_{tx} - Z_c + Z_c)||(-Z_c + Z_{rx} + R_L) \\ Z_{21,ef} = Z_c\left[\dfrac{R_L}{R_L + Z_{rx}}\right] \end{cases} \tag{15}$$

where Z_{tx} and Z_{rx} represent the impedance of the *tx* coil and *rx* coil, respectively, and R_L is the load resistance of the receiving circuit. Consistent with [27], the WPT efficiency (η) can be computed from the system Z-parameters as shown in Eq. (16).

$$\eta = \frac{|Z_{21,\text{ef}}|^2}{\Re\{Z_{11,\text{ef}}\}R_L} \times 100 \quad [\%]. \tag{16}$$

The above derivation is chosen due to its simplicity and explicit dependence on Z-parameters. As would later be described in section V, the Z-parameters are extracted using the experimental testbench in Figure 11 while using an optimal value of R_L to maximize the power transfer efficiency. Moreover, it is worth mentioning that the derived 2-port model is equally valid and applicable for estimating the PTE of an MM-based WPT system, incorporating a metamaterial between the coils. When integrated with MM, however, it is expected that some power will be stored in the near field of the MM even when the *Tx* and *Rx* coils are self-resonant. While a complex power can be drawn from the circuit, the reactive component needs to be removed from the efficiency calculation since it is not dissipated in the circuit.

V. PROTOTYPE TEST-BED AND EXPERIMENTAL INVESTIGATION

In this section, a prototype test sample of the proposed MM was fabricated for experimental measurement and performance validation of the proposed metamaterial design. To this end, both the MM unit cell and MM-slab (4×4 unit cell array) were fabricated with a 26 AWG single-strand copper wires using PCB technology. Subsequently, the fabricated structure was posited on a $1mm$ thick FR4 substrate to safely secure the copper wires as shown in Figure 10. Furthermore, compensation capacitors were soldered underneath the board in accordance with the specification in Table 2. In addition, the *Tx*-coil and *Rx*-coil were respectively connected to port 1 and port 2 of the Keysight EN5061A vector network analyzer (VNA), using 50Ω micro SMA connectors. Finally, the substrate slab was provided with external holes, allowing for support and positioning framework for the experimental set-up.

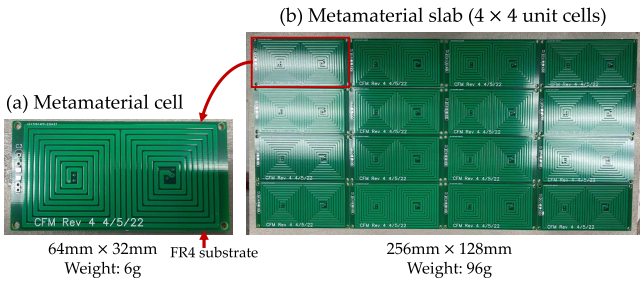

FIGURE 10. Fabricated prototype of the proposed metamaterial (MM).

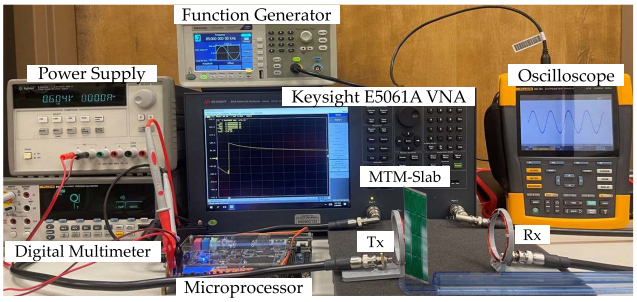

FIGURE 11. Experimental test-bed of the proposed metamaterial-based WPT system showing the Keysight ENA 5061A VNA and the circuit structure.

Concretely, port 1 and port 2 were utilized for measuring the S-parameters (transmission coefficient S_{21}, and reflection coefficient, S_{11}) and the Z-parameters. Going forward, the fabricated MM-slab was integrated with an equivalent coil design consisting of a *Tx*- coil and *Rx*- coil. To preserve the working distance/loading position, the distance between the *Tx*-coil and MM-slab was fixed at $1mm$ (see Figure 11) while taking measurements for sweep values of the working distance (distance between *Rx*-coil and MM-slab) ranging from $10mm$ to $50mm$. Afterward, a stimulus with a start frequency of 100kHz (0.1MHz), a stop frequency of 10MHz, and 671 data points was harnessed for the coil excitation. For each working distance, the corresponding scattering parameters (S_{21} and S_{11}), and Z-parameters were extracted and utilized in subsequent analysis to compute the power transfer efficiency (PTE) of the proposed system. Further, a preliminary study of the mutual coupling (Z_c) and PTE is conducted based on the extracted Z-parameters. For the purposes of performance comparison, the same experimental procedure was performed on the WPT system without inserting the MM-slab.

VI. EXPERIMENTAL RESULTS AND PERFORMANCE ANALYSIS

Using the above experimental set-up, the generated measurement waveforms for transmission coefficient (S_{21}) and reflection coefficient (S_{11}) is exhibited in Figure 12(a) and Figure 12(b), respectively. Both measurements results indicate the proposed MM resonates at a frequency of 743.5kHz, which is significantly low compared to the resonant frequency of existing metamaterial designs in published

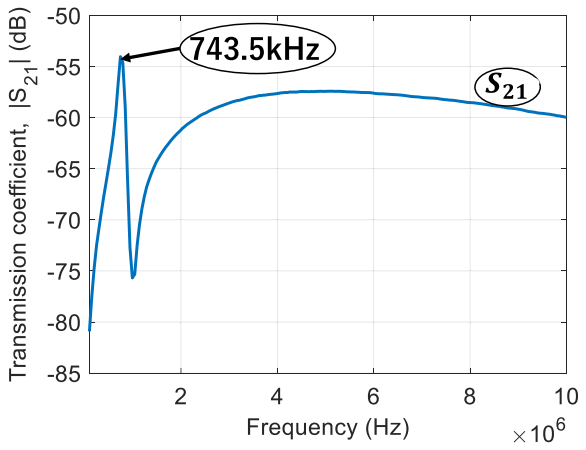

(a) Transmission coefficient, S_{21}

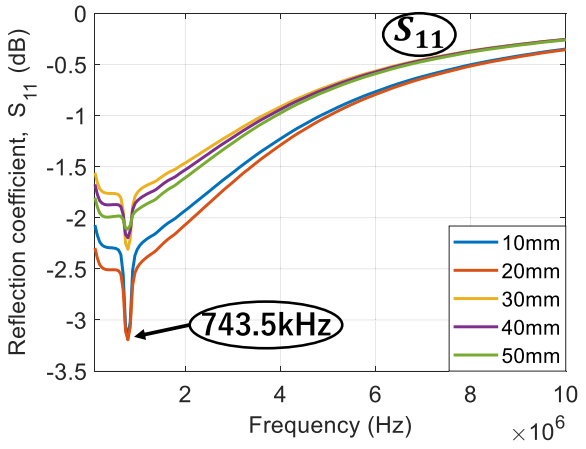

(b) Reflection coefficient, S_{11}

FIGURE 12. Measurement waveform of forward transmission (S_{21}) and reflection (S_{11}) coefficients of the proposed metamaterial unit cell using Keysight E5061A ENA VNA. The MM structure shows a negative real value of μ_f at the resonant frequency, F_r = 745.5kHz.

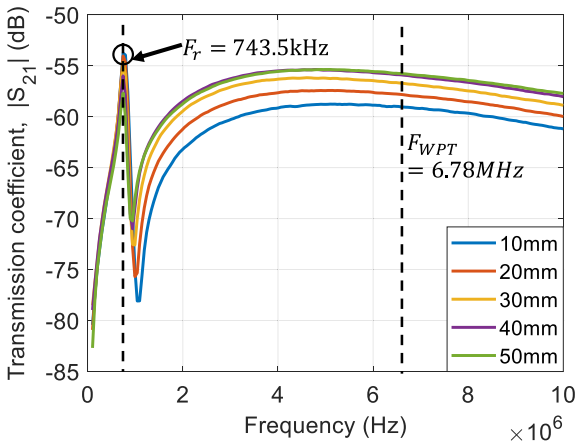

FIGURE 13. Measured magnitude waveform of forward transmission coefficients (S_{21}) and reflection coefficient (S_{11}), considering a transmitter to Meta-material distance of 20*mm*. The resonant frequency of 743.5kHz is observed consistent with Fig. 12.

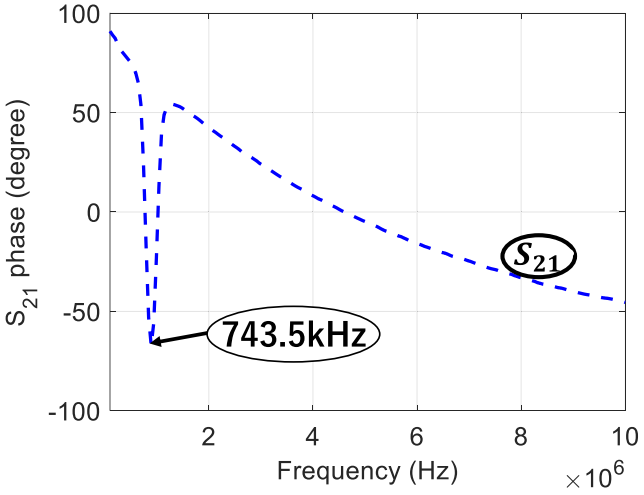

FIGURE 14. Measured phase plot of forward transmission coefficient (S_{11}) considering 30*mm* transmitter to Meta-material distance. The resonant frequency of 743.5kHz is observed.

literature. Furthermore, when the transmitter (Tx) to meta-material (MM) distance is fixed at 1mm (to preserve the working distance), and the loading position of the Rx- coil relative to MM is varied from 10mm to 50mm as exemplified in Figure 12(b) and Figure 13, the MM obviously resonates at a reasonably constant frequency ($F_r \approx 743.5kHz$) while its magnitude becomes smaller as the loading position increases. Essentially, while the magnitude of S_{21} and S_{11} largely depends on the loading position, it has no appreciable effect on the resonant operating frequency.

Going forward, Figure 14 shows the phase plot of S_{21}, demonstrating the same resonant frequency (743.5kHz) as the magnitude plot. As seen in Figure 15, when the Tx to MM distance is fixed at 1mm (to preserve the working distance), and the loading position (Rx to MM distance) is swept from 10mm to 50mm, the notable decrease in phase angle is observed as the loading position increases. Nonetheless, the resonant frequency remains constant at 743.5kHz independent of the loading position. Thus, it can be deduced that while the loading position significantly impacts the reactive parameters of the structure, it has no appreciable effect on it's resonant frequency. In practice, the incorporation of MM-slab introduces a phase shift, arising from the reactive parameters of the MM sample. Given the complex nature of the MM (more resonant cells) compared to a standard WPT system, it is expected that the resonant frequency of the device will be sensitive to variations in material composition and geometrical parameters [28]. Essentially, the demonstrated low resonance frequency of the MM sample can effectively limit the overall power dissipation in the WPT system by reducing the switching losses on the power switches while also limiting the voltage and current stresses in the passive components and power electronics. Meanwhile, the corresponding effective permeability (μ_f) waveform of the proposed metamaterial is exhibited in Figure 16. Consistent with the S_{21} and S_{11} waveforms, the μ_f waveform clearly shows the metamaterial resonating at a frequency of 743.5kHz.

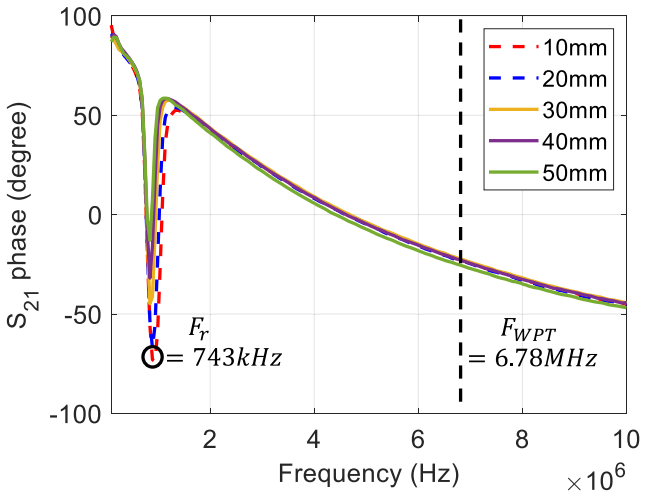

FIGURE 15. Measured S_{21} phase plot for working distance (MM to receiver) ranging form 10*mm* to 50*mm*. A constant resonant frequency F_r= 743kHz is indicated for varying loading positions.

Besides, at F_r= 743kHz, a corresponding negative real value of μ_f is observed, effectively characterizing the proposed metamaterial structure.

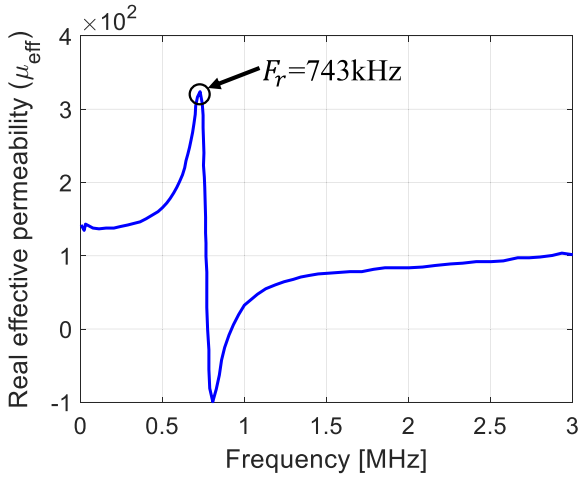

FIGURE 16. Plot of effective permeability (μ_f) versus frequency for a unit MM cell. A negative real value of μ_f at the resonant frequency, F_r = 743kHz characterizes the MM (a) real effective permeability, μ_f .

Lastly, a comparison waveform showing the magnitude of S_{21} versus transfer distance for both simulation and experimental measurement is exhibited in Figure 17. Based on the waveform, it is apparent that the simulation results closely match the experimental measured results, effectively validating the feasibility of the proposed equivalent circuit model in verifying the transfer characteristics of the proposed MM-based WPT system. While the simulation magnitude of S_{21} is slightly larger than its calculated counterpart, the slight disparity can be attributed to the inherent approximation in the model analysis. Further, it is notable that both the simulated and measured magnitude of S_{21} attains maximum

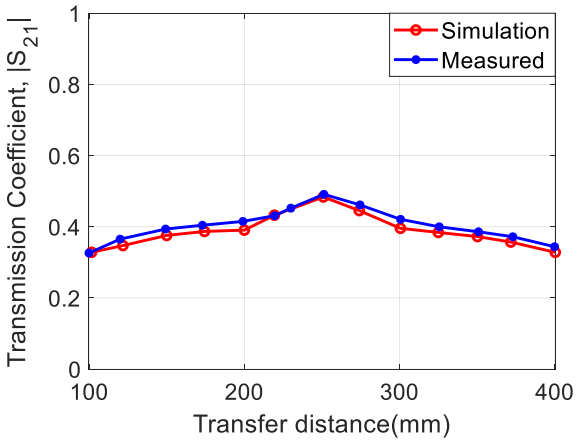

FIGURE 17. Comparison waveform of measured and simulated forward transmission coefficient (S_{21}) versus transfer distance (MM to *Rx* distance). Model simulation is based on Finite Element Analysis in ANSYS HFSS.

value when the MM is placed 250*mm* away from the *Rx* coil. This represents the optimal position of the MM-slab.

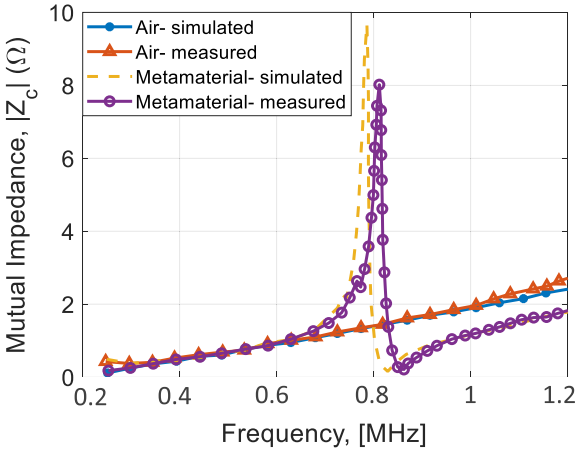

FIGURE 18. Comparison of experimental/measured and simulated mutual impedance (Z_c) with and without using MM-slab. The peak mutual impedance for the simulation and measurement corresponds to 790kHz and 810kHz resonance frequencies, respectively.

A. MUTUAL IMPEDANCE, Z_c

Figure 18 shows a comparison of the mutual coupling (Z_c) for the WPT system with and without metamaterial at the operating frequency. In order to maintain equal working distance in the two cases, the position, and thickness of the MM-slab was taken into account while measurements were taken for each step increase in working distance and operating frequency. Concretely, the metamaterial-based system outperforms the magnitude of the mutual coupling values obtained using the conventional Tx/Rx system, attaining its peak at the resonant operating frequency. Thus, the validity of the overall design coupled with the effectiveness of the metamaterial in enhancing the convergence of magnetic field at the receiver is demonstrated. Besides, both the simulation and experimental results demonstrate close matching, albeit with a slight dif-

ference in resonance frequency (790kHz for simulation and 805kHz for measurement using MM). While on the one hand the frequency shift could be attributed to capacitive effects and design approximations due to manufacturing tolerances; on the other hand, the lower amplitude value is due to the additional losses from the fabrication process. By and large, it should be noted that the increase in mutual coupling is wholly due to the evanescent wave amplification property of the metamaterial which engenders a coupling and convergence of near magnetic field, leading to reduced leakage electromagnetic field. Furthermore, Figure 19 shows a close matching of the simulated and measured Z_c as a function of transfer distance for the WPT system with and without MM. In comparison to the Tx/Rx coil without MM, the WPT system using MM engenders higher mutual coupling for all normalized distances, leading to enhanced mutual impedance.

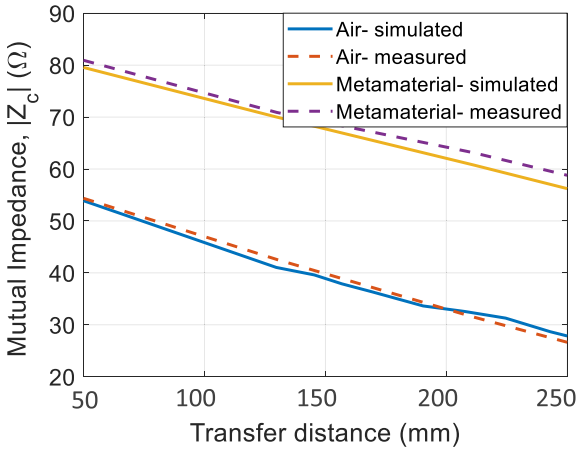

FIGURE 19. Comparison of experimental/measured and simulated mutual impedance (Z_c) against transfer distance with and without using MM-slab.

B. POWER TRANSFER EFFICIENCY, η

In this section, the experimentally extracted Z-parameters based on the prototype set-up elucidated in section V (Fig. 11) were applied to (16) to evaluate the power transfer efficiency (PTE). For comparison purposes, measurements were taken for the same loading positions (MM to receiver distance) as ANSYS electromagnetic simulation. Fig. 20 shows the simulated and measured waveform of PTE against normalized distance ($\frac{d_x}{d}$) for the system with and without MM. The normalized distance is based on the ratio of the maximum working distance (d_w) equivalent to the distance between Rx coil and MM-slab and parametric working distance (d) considered in the simulation. Ostensibly, the simulation and measured PTE are closely matched, the slight difference being caused by some approximation in the computation of the lumped element impedances. In addition, when the MM-slab is integrated with the WPT system, the PTE increases significantly for the entire normalized distances in comparison to the original system without metamaterial. Using the normalized distance, 2, as a case in point, it is observed that the PTE

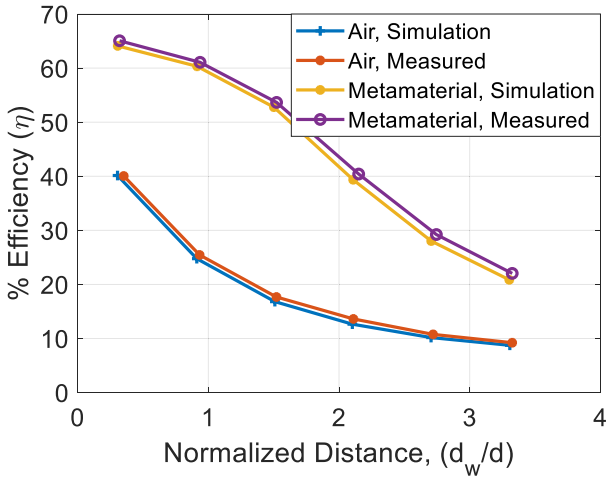

FIGURE 20. Comparison of simulated and measured transfer efficiency of the WPT system with and without metamaterial. The normalized distance is based on the ratio of the maximum transfer distance and parametric transfer distances ($\frac{d_w}{d}$) considered for the full-wave simulation.

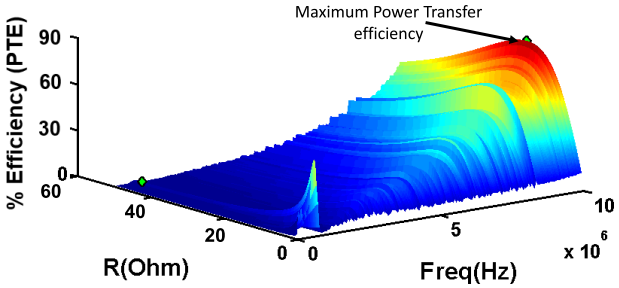

FIGURE 21. 3D rendering of power transfer efficiency based on option 006 WPT analysis toolbox in Keysight ENA 5061A VNA. The 3D plot is represented as a function of the load resistance and frequency sweeps.

increases from 12% (for the original system without MM) to 40% (for the MM-based system), representing a 28% increase in PTE. The above increase in efficiency can be explained through a careful analysis of the efficiency expression in Eq. (16). Apparently, the WPT efficiency demonstrates a square dependence on $|Z_{21,ef}|$, which is a linear function of the mutual impedance, Z_c. In general, the mutual coupling and efficiency of a conventional two coil WPT system decays exponentially as the cube inverse of the working distance, ($\approx 1/d_w^3$) whereas, with the insertion of MM, the mutual impedance, Z_c is significantly enhanced, leading to greater improvement in efficiency. The result further accentuates the effectiveness of the proposed MM in enhancing evanescent wave amplification, mutual coupling of near magnetic field, and WPT efficiency.

Additionally, the option 006 WPT analysis feature in Keysight E5061A VNA offers additional capability for real time measurement and 2D/3D visualization of power transfer efficiency using arbitrarily variable impedances. For the purpose of this analysis, the reactance, X, was fixed while R_L was swept from 10Ω to 60Ω, and the frequency from 100kHz to 10MHz. The resulting 3D waveform of power transfer efficiency is depicted in Fig. 21. As indicated by the arrow

line, the maximum PTE of the WPT system corresponds to 80%. Following these measurement results, it is experimentally verified that the proposed thin PCB-type metamaterial with negative effective permeability highly enhances the performance of the WPT system through a confinement and coupling of near magnetic field.

VII. CONCLUSION

In this study, a low-frequency metamaterial coupled with an equivalent circuit model has been investigated to explore the performance and transfer characteristics of metamaterial-based WPT system. In addition, a model-based approach for extracting medium parameters, including effective permeability and scattering parameters have been explicitly investigated. The circuit parameters are obtained by numerical calculation, and Finite Element Analysis (FEA) coupled with experimental measurement to validate the system performance. Essentially, both the simulation and measurement results closely demonstrate the proposed meta-material resonating at a low frequency (745kHz) which is significantly low compared to the GigaHertz and Mega-Hertz resonant frequencies of existing MM structures. Concretely, the performance comparison between the simulation results and experimental measurement effectively verifies the validity of the proposed system. While 743kHz is relatively low compared to the microwave and radio frequency of existing MM structures, this frequency can be further mitigated to ensure efficient operation of power switches with minimal switching losses. Thus, as a future extension of this work, the utilization of optimization algorithm can be explored to optimize the physical param- eters of the metamaterial, potentially lowering the resonant frequency to 85kHz range, compatible with conventional WPT system. To the best of the authors' knowledge, this paper has profound significance for subsequent theoretical investigation of metamaterial-based WPT system while offering the potential to drive future industrial applications.

REFERENCES

[1] V. T. Nguyen, S. H. Kang, and C. W. Jung, "Wireless power transfer for mobile devices with consideration of ground effect," in *Proc. IEEE Wireless Power Transf. Conf. (WPTC)*, May 2015, pp. 1–4.

[2] A. K. Ramrakhyani, S. Mirabbasi, and M. Chiao, "Design and optimization of resonance-based efficient wireless power delivery systems for biomedical implants," *IEEE Trans. Biomed. Circuits Syst.*, vol. 5, no. 1, pp. 48–63, Feb. 2011.

[3] W. Adepoju, I. Bhattacharya, M. Sanyaolu, M. E. Bima, T. Banik, E. N. Esfahani, and O. Abiodun, "Critical review of recent advancement in metamaterial design for wireless power transfer," *IEEE Access*, vol. 10, pp. 42699–42726, 2022.

[4] W. O. Adepoju, I. Bhattacharya, M. E. Bima, and T. Banik, "Novel metamaterial and AI-based multi-objective optimization of coil parameters for efficient wireless power transfer," in *Proc. IEEE Vehicle Power Propuls. Conf. (VPPC)*, Oct. 2021, pp. 1–6.

[5] J. B. Pendry, "Negative refraction makes a perfect lens," *Phys. Rev. Lett.*, vol. 85, no. 18, pp. 3966–3969, Oct. 2000.

[6] E. S. G. Rodríguez, A. K. RamRakhyani, D. Schurig, and G. Lazzi, "Compact low-frequency metamaterial design for wireless power transfer efficiency enhancement," *IEEE Trans. Microw. Theory Techn.*, vol. 64, no. 5, pp. 1644–1654, May 2016.

[7] H. Kim and C. Seo, "Highly efficient wireless power transfer using metamaterial slab with zero refractive property," *Electron. Lett.*, vol. 50, no. 16, pp. 1158–1160, 2014.

[8] G. Lipworth, J. Ensworth, K. Seetharam, D. Huang, J. S. Lee, P. Schmalenberg, T. Nomura, M. S. Reynolds, D. R. Smith, and Y. Urzhumov, "Magnetic metamaterial superlens for increased range wireless power transfer," *Sci. Rep.*, vol. 4, no. 1, pp. 1–6, Jan. 2014.

[9] A. L. A. K. Ranaweera, T. P. Duong, and J.-W. Lee, "Experimental investigation of compact metamaterial for high efficiency mid-range wireless power transfer applications," *J. Appl. Phys.*, vol. 116, no. 4, Jul. 2014, Art. no. 043914.

[10] T. C. Beh, M. Kato, T. Imura, S. Oh, and Y. Hori, "Automated impedance matching system for robust wireless power transfer via magnetic resonance coupling," *IEEE Trans. Ind. Electron.*, vol. 60, no. 9, pp. 3689–3698, Sep. 2013.

[11] Y. Urzhumov and D. R. Smith, "Metamaterial-enhanced coupling between magnetic dipoles for efficient wireless power transfer," *Phys. Rev. B*, vol. 83, no. 20, May 2011.

[12] F. Bilotti, A. Toscano, L. Vegni, K. Aydin, K. B. Alici, and E. Ozbay, "Equivalent-circuit models for the design of metamaterials based on artificial magnetic inclusions," *IEEE Trans. Microw. Theory Techn.*, vol. 55, no. 12, pp. 2865–2873, Dec. 2007.

[13] Y. Cho, S. Lee, D.-H. Kim, H. Kim, C. Song, S. Kong, J. Park, C. Seo, and J. Kim, "Thin hybrid metamaterial slab with negative and zero permeability for high efficiency and low electromagnetic field in wireless power transfer systems," *IEEE Trans. Electromagn. Compat.*, vol. 60, no. 4, pp. 1001–1009, Aug. 2018.

[14] K. B. Alici, F. Bilotti, L. Vegni, and E. Ozbay, "Miniaturized negative permeability materials," *Appl. Phys. Lett.*, vol. 91, no. 7, Aug. 2007, Art. no. 071121.

[15] B. Wang, K. H. Teo, T. Nishino, W. Yerazunis, J. Barnwell, and J. Zhang, "Experiments on wireless power transfer with metamaterials," *Appl. Phys. Lett.*, vol. 98, no. 25, p. 254101, Jul. 2011.

[16] Y. Zhao, V. Vutipongsatorn, and E. Leelarasmee, "Improving the efficiency of wireless power transfer systems using metamaterials," in *Proc. 10th Int. Conf. Electr. Eng./Electron., Comput., Telecommun. Inf. Technol.*, May 2013, pp. 1–4.

[17] W.-C. Chen, C. M. Bingham, K. M. Mak, N. W. Caira, and W. J. Padilla, "Extremely subwavelength planar magnetic metamaterials," *Phys. Rev. B*, vol. 85, no. 20, May 2012.

[18] J.-F. Chen, Z. Ding, Z. Hu, S. Wang, Y. Cheng, M. Liu, B. Wei, and S. Wang, "Metamaterial based high efficiency wireless power transfer system at 13.56 MHZ for low power application," *Prog. Electromagn. Res. B*, vol. 72, pp. 17–30, 2017.

[19] D. Brizi, N. Fontana, S. Barmada, and A. Monorchio, "An accurate equivalent circuit model of metasurface-based wireless power transfer systems," *IEEE Open J. Antennas Propag.*, vol. 1, pp. 549–559, 2020.

[20] C. Hoer and C. Love, "Exact inductance equations for rectangular conductors with applications to more complicated geometries," *J. Res. Nat. Bur. Standards, Sect. C, Eng. Instrum.*, vol. 69C, no. 2, p. 127, Apr. 1965.

[21] Z. Luo and X. Wei, "Analysis of square and circular planar spiral coils in wireless power transfer system for electric vehicles," *IEEE Trans. Ind. Electron.*, vol. 65, no. 1, pp. 331–341, Jan. 2018.

[22] Y. Cho, J. J. Kim, D.-H. Kim, S. Lee, H. Kim, C. Song, S. Kong, H. Kim, C. Seo, S. Ahn, and J. Kim, "Thin PCB-type metamaterials for improved efficiency and reduced EMF leakage in wireless power transfer systems," *IEEE Trans. Microw. Theory Techn.*, vol. 64, no. 2, pp. 1–12, Jan. 2016.

[23] H. Kim, C. Song, J. Kim, J. Kim, and J. Kim, "Shielded coil structure suppressing leakage magnetic field from 100W-class wireless power transfer system with higher efficiency," in *IEEE MTT-S Int. Microw. Symp. Dig.*, May 2012, pp. 83–86.

[24] Z. Szabo, G.-H. Park, R. Hedge, and E.-P. Li, "A unique extraction of metamaterial parameters based on Kramers–Kronig relationship," *IEEE Trans. Microw. Theory Techn.*, vol. 58, no. 10, pp. 2646–2653, Oct. 2010.

[25] A. W. Oluwafemi, E. Ozsoy, S. Padmanaban, M. S. Bhaskar, K. V. Ramachandaramurthy, and V. Fedak, "A modified high output-gain Cuk converter circuit configuration for renewable applications—A comprehensive investigation," in *Proc. IEEE Conf. Energy Convers. (CENCON)*, Oct. 2017, pp. 117–122.

[26] Y. P. Su, X. Liu, and S. Y. R. Hui, "Mutual inductance calculation of movable planar coils on parallel surfaces," *IEEE Trans. Power Electron.*, vol. 24, no. 4, pp. 1115–1123, Apr. 2009.

[27] A. K. RamRakhyani and G. Lazzi, "On the design of efficient multi-coil telemetry system for biomedical implants," *IEEE Trans. Biomed. Circuits Syst.*, vol. 7, no. 1, pp. 11–23, Feb. 2013.
[28] V. Cirimele, R. Torchio, J. L. Villa, F. Freschi, P. Alotto, L. Codecasa, and L. D. Rienzo, "Uncertainty quantification for SAE J2954 compliant static wireless charge components," *IEEE Access*, vol. 8, pp. 171489–171501, 2020.

WEBSTER ADEPOJU (Graduate Student Member, IEEE) received the Bachelor of Science degree in electrical and electronic engineering from Obafemi Awolowo University, Nigeria, and the Master of Engineering degree (Hons.) in electrical and electronic engineering from the University of Johannesburg (UJ), South Africa. He is currently pursuing the Ph.D. degree in electrical and computer engineering with the SOLBAT-TTU Energy Research Laboratory, Tennessee Technological University, USA. From 2018 to 2019, he was a Research Assistant with the Centre for Telecommunication, UJ, where he has investigated the effect of common mode and differential mode noise on cables used for power line communication. Prior to this, he has worked on the modeling and control of high-gain DC–DC converters, observer-based sensor-less systems, and advanced model predictive control of single phase inverter. His current research interests include low frequency metamaterial-based wireless power transfer, power electronics, wide band gap devices, and semiconductor modeling. He was a recipient of the 2021 Best Poster Presentation Award at the University's Research and Creative Inquiry Day.

INDRANIL BHATTACHARYA (Senior Member, IEEE) received the Bachelor of Engineering degree (Hons.) in electronics and communication engineering from India and the M.S. and Ph.D. degrees in electrical engineering from Florida State University. He is currently an Associate Professor (tenured) with the Electrical and Computer Engineering Department, Tennessee Tech University. He is the main inventor of two U.S. patents. He has been the Principal or a Co-Principal Investigator of USD 2.5 Million funding from agencies, like the National Science Foundation, the U.S. Department of Energy, and the Oak Ridge National Laboratory. He has published 43 peer-reviewed technical papers in reputed journals and conferences. He has supervised seven Ph.D., 11 master's, and 50 undergraduate students. His research interests include lithium and sodium-based battery technologies, high-efficiency III–V solar cells, wireless power transfer, and electromagnetics.

MARY SANYAOLU received the bachelor's degree from the University of Lagos and the master's degree from the University of Johannesburg, South Africa. From 2014 to 2015, she was an Intern with Oando Oil Corporation. She was with the University of Johannesburg, from 2017 to 2021. She is currently a Geo-Technical Engineer at GasFleet Engineering Ltd. Her current research interests include nanomaterials and material characterization, modeling, and analysis. She was a recipient of the prestigious Global Excellence Scholarship and the National Research Fellowship.

EBRAHIM NASR ESFAHANI (Student Member, IEEE) received the B.S. degree in electrical engineering from Kashan University, Iran, in 2007, and the M.S. degree in electrical engineering from IAUN, Iran, in 2010. He is currently pursuing the Ph.D. degree in electrical and computer engineering with Tennessee Technological University, Cookeville, TN, USA. He was in the industry as an Electrical Maintenance Engineer at the steel company for more than eight years. His research interests include design and analysis of electric machines, modeling of electromagnetic devices, and wireless power transfer.